PCCP

PAPER

View Article Online
View Journal

Cite this: DOI: 10.1039/c8cp03782e

Thermodynamics of Sr_2NiMoO_6 and Sr_2CoMoO_6 and their stability under reducing conditions†

V. V. Sereda,*[a] D. S. Tsvetkov,[a] A. L. Sednev,[a] A. I. Druzhinina,[b] D. A. Malyshkin[a] and A. Yu. Zuev[a]

Received 14th June 2018,
Accepted 16th July 2018

DOI: 10.1039/c8cp03782e

rsc.li/pccp

The values of standard enthalpy of formation at 298.15 K and 1 atm for the double perovskites Sr_2NiMoO_6 and Sr_2CoMoO_6, measured by means of drop solution calorimetry, were found to be -2418.1 ± 12.4 and -2422.9 ± 9.6 kJ mol^{-1}, respectively. Heat capacity of Sr_2NiMoO_6 and Sr_2CoMoO_6 was measured between 2 and 370 K using relaxation and adiabatic calorimetry, and the enthalpy increments – between 373 and 1273 K using drop calorimetry. Low-temperature magnetic and higher-temperature structural phase transformations in Sr_2NiMoO_6 and Sr_2CoMoO_6 were discussed from the thermodynamic point of view. Specific heat (C_p), standard enthalpy ($\Delta_0^T H^0$) and standard entropy (S^0) functions were derived from the experimental data for both double perovskites. The values of C_p, $\Delta_0^T H^0$ and S^0 at 298.15 K were determined to be 202.31 ± 0.61 J mol^{-1} K^{-1}, 36.12 ± 0.18 kJ mol^{-1} and 231.3 ± 1.6 J mol^{-1} K^{-1} for Sr_2NiMoO_6, and 212.66 ± 0.64 J mol^{-1} K^{-1}, 38.25 ± 0.19 kJ mol^{-1} and 244.4 ± 1.7 J mol^{-1} K^{-1} for Sr_2CoMoO_6, respectively. Additionally, using the thermodynamic data available, phase diagrams with respect to T and p_{O_2} showing stability limits and decomposition products were calculated for Sr_2NiMoO_6 and Sr_2CoMoO_6. Though the cobaltite's stability range is wider than nickelate's both in terms of T and p_{O_2}, both complex oxides were found to be stable only at reasonably high temperatures and in oxidizing conditions, and metastable at low temperatures.

1. Introduction

Complex oxides Sr_2CoMoO_6 and Sr_2NiMoO_6 belong to a family of rock-salt-ordered double perovskites with elpasolite-like structure. An interested reader is referred to the work of Vasala and Karppinen[1] for the extensive review of the $A_2BB'O_6$ compounds with similar crystal structure. Both Sr_2CoMoO_6 and Sr_2NiMoO_6 had first been synthesized and characterized in 1960s,[2,3] but their properties received closer attention only a few decades later. Earlier studies were focused on the low-temperature properties of Sr_2CoMoO_6 and Sr_2NiMoO_6.[3–9] It was found that both oxides, being magnetoelectric multiferroics, are capable of the long-range ordering of magnetic and electric dipoles.[4,7,9,10] Because of the rock-salt ordering, magnetically active Co and Ni cations are separated by MoO_6 octahedra with supposedly high level of covalent bonding. Hence, the antiferromagnetism in Sr_2CoMoO_6 and Sr_2NiMoO_6 is due to the long-range superexchange interactions *via* the M–O–Mo–O–M (M = Co, Ni) pathways.[1,4,9]

The attempts to alter the magnetic properties by changing the oxygen nonstoichiometry of Sr_2CoMoO_6 first raised the question of the chemical stability of this oxide.[5,8] The issues of stability and chemical compatibility with the state-of-the-art solid oxide fuel cell (SOFC) electrolytes became more pressing in the later studies where the suitability of both Sr_2CoMoO_6 and Sr_2NiMoO_6 as SOFC anode materials was investigated. Concerning these matters, contradictory findings were reported for both oxides. For example, Viola *et al.*[5] observed no decomposition of Sr_2CoMoO_6 in 15% H_2/N_2 at 1123 K, whereas the other authors point out its decomposition temperature in 5% H_2/N_2 to be 1123 K[11] or even as low as 1073 K.[9,12–15] Similar disagreement between the authors' results exists for Sr_2NiMoO_6 – Wei *et al.*[16] synthesized it successfully at 1373 K in 5% H_2/N_2, but the other authors reported the onset of its decomposition to be at 1073 K (in the same atmosphere).[9,12–15] Furthermore, among the products of reduction of Sr_2CoMoO_6 and Sr_2NiMoO_6 in H_2 atmosphere different strontium molybdates were detected in different works – $SrMoO_4$,[9,11] $SrMoO_3$,[12,14] Sr_2MoO_4,[12] Sr_3MoO_6.[12,14,17]

Summarizing reported results, it seems to be unlikely that Sr_2CoMoO_6 or Sr_2NiMoO_6 is stable even at 1073 K in 5% H_2/N_2, with Sr_3MoO_6 being the most probable decomposition product. However, this conclusion does not eliminate the existing

---

[a] *Department of Physical and Inorganic Chemistry, Institute of Natural Sciences and Mathematics, Ural Federal University, 620002, 19 Mira st., Yekaterinburg, Russia. E-mail: vladimir.sereda@urfu.ru*

[b] *Department of Chemistry, Moscow State University, 119991, GSP-1, 1-3 Leninskiye Gory, Moscow, Russia*

† Electronic supplementary information (ESI) available. See DOI: 10.1039/c8cp03782e

contradictions in the reported data. Moreover, the available discrepant data, obtained as a result of the short-term annealing experiments, cannot provide any sound information on the potential long-term chemical stability of Sr_2CoMoO_6 or Sr_2NiMoO_6 under the given conditions. It is beyond doubt that such information is of great importance for successful practical application of these oxides, because both their magnetic properties[5,8,12] and anode performance can be altered significantly by partial reduction and/or decomposition of the oxides. As for the latter, it was shown that controlled partial decomposition of Sr_2CoMoO_6 or Sr_2NiMoO_6, resulting in the cermet formation, can be rather beneficial for the electrical conductivity of the as-obtained anode material.[12,14]

It is evident that the fundamental thermodynamic data can clarify the stability and chemical compatibility issues for the double perovskites of interest. Meanwhile, heat capacities of Sr_2CoMoO_6 and Sr_2NiMoO_6 were measured only by Gunjikar *et al.*[18] in relatively narrow temperature range, 290–580 K. In view of the existence of low-temperature antiferromagnetic phase transitions in both oxides, low-temperature heat capacity data is crucial for the correct entropy determination. Such data, as well as the formation enthalpies, and the high-temperature thermodynamic properties of either Sr_2CoMoO_6 or Sr_2NiMoO_6, have not been reported yet. Therefore, the present work was aimed to obtain the complete set of thermodynamic properties such as heat capacity, standard entropy, enthalpy and Gibbs energy of formation for Sr_2CoMoO_6 and Sr_2NiMoO_6 in wide temperature range. The data obtained were used for the evaluation of thermodynamic stability of both double perovskites under reducing conditions.

2. Experimental

2.1. Preparation and characterization of samples

Double perovskites Sr_2CoMoO_6 and Sr_2NiMoO_6 were synthesized *via* the standard ceramic technique. High-purity $SrCO_3$, NiO, Co_3O_4, and $(NH_4)_6Mo_7O_{24}·4H_2O$ (see Table 1 for details) were used as starting materials. Stoichiometric mixtures of corresponding precursors were annealed consecutively at temperatures 873–1373 K in air with 100 K steps and intermediate regrindings. Resulting powders were uniaxially pressed and then calcined at 1623 K in air. The dwell time at each firing stage was at least 10 h. Phase composition of as-sintered double perovskites was determined by Equinox 3000 diffractometer (Inel, France) using Cu Kα radiation. X-ray diffraction (XRD) patterns for Sr_2CoMoO_6 and Sr_2NiMoO_6 were indexed in *I*4/*m* space group[6,7] and, as seen in Fig. 1, showed no indication for the presence of a second phase.

Table 1 Chemical compounds used in the present work

Chemical name	Source	Mass fraction purity	Analysis method
NiO	UZKhR	>0.9999	—
MoO_3	Vekton	>0.99	—
$(NH_4)_6Mo_7O_{24}·4H_2O$	Khimreaktivsnab	>0.99	—
$SrCO_3$	Vekton	>0.999999	—
Co_3O_4	MCP HEK GmbH	>0.9997	—
CoO	Synthesis	>0.99	XRD, AAS[a]
Sr_2CoMoO_6	Synthesis	>0.99	XRD, AAS
Sr_2NiMoO_6	Synthesis	>0.99	XRD, AAS
Sapphire (α-Al_2O_3)	Setaram	>0.9995	—
Au	Setaram	>0.9999	—
Ar (gas)	Uralkriogas	>0.99998	—

[a] Atomic absorption spectroscopy.

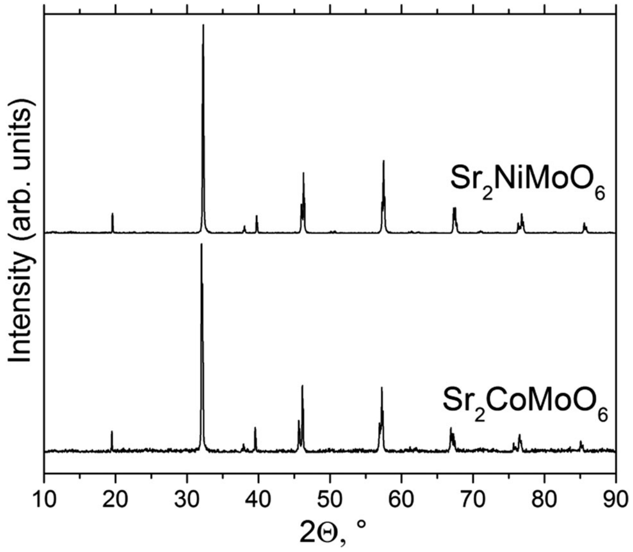

Fig. 1 X-ray diffraction patterns for Sr_2CoMoO_6 and Sr_2NiMoO_6.

More or less dense samples that cannot be crumbled easily are more convenient to handle in the drop calorimetry. However, the samples with high density may not dissolve rapidly in viscous melts, which are used for drop solution experiments. In order to obtain dense enough precursor pieces, 10–20 mg of which could dissolve completely in the borate melt within at least 30 min, corresponding powders had been uniaxially pressed and then were treated differently.

Nickel oxide NiO used for calorimetric measurements was preliminarily annealed at 973 K in air.

Molybdenum oxide MoO_3, which is highly volatile, was calcined at 1023 K in a quartz tube.

It is known that cobalt attains an oxidation state +2 in borate melts[19] and, therefore, CoO was used in the drop solution experiments. Cobalt monoxide CoO was obtained by annealing Co_3O_4 pellet at 1273 K in the atmosphere with low p_{O_2} (10^{-5} atm). Annealed pellet was rapidly quenched to room temperature.

To avoid the decomposition of strontium carbonate $SrCO_3$, it was sintered in atmosphere of pure CO_2 at 1273 K with subsequent annealing at 1073 K for 24 h. The final annealing temperature was specifically chosen to be less than 1197 K since the transition of orthorhombic $SrCO_3$ to hexagonal one occurs at this temperature.[20] This technique allowed us to obtain dense pellet of single-phase orthorhombic $SrCO_3$.

All the compounds used in the present work are listed in Table 1.

2.2. Differential scanning calorimetry (DSC)

In order to investigate the heat effects of the phase transitions in Sr_2CoMoO_6 and Sr_2NiMoO_6 in the range 330–873 K, DSC measurements were performed using STA 409 PC Luxx (Netzsch, Germany). The experiments were carried out in the flow of argon (30 ml min^{-1}) with 10 K min^{-1} heating rate. Simultaneous thermogravimetric (TG) measurements showed no mass loss, indicating no deviation from stoichiometry for both samples in the whole temperature range investigated.

2.3. Low-temperature relaxation calorimetry

Low-temperature heat capacity of Sr_2CoMoO_6 and Sr_2NiMoO_6 was measured at temperatures from 2 to 100 K using Physical Property Measurement System (PPMS) by Quantum Design, USA. In order to subtract the contributions of sample holder and Apiezon N vacuum grease, blank experiments (without the sample) were performed in advance. Then small (around 5–10 mg) amounts of oxides in the form of dense pieces, weighted with high precision, were placed directly on the greased sample platform. Based on the prior experience, experimental error of the heat capacity determination is estimated to be less than 2%.

2.4. Low-temperature vacuum adiabatic calorimetry

The heat capacity of the samples in the temperature range from 80 to 370 K was measured using an automated vacuum adiabatic calorimeter with liquid nitrogen as refrigerant. Device configuration and calorimetric technique were described in detail by Varushchenko *et al.*[21] The heat capacity was measured in a heating mode with 1 K steps. The sample container was filled with helium (p_{He}(298 K) = (10 ± 2) kPa) which served as a thermal exchange gas. High vacuum inside the calorimetric cell was kept by means of cryosorption provided with an efficient charcoal getter. Around 1.5 g and 2.2 g of Sr_2CoMoO_6 and Sr_2NiMoO_6, respectively, were used for the measurements. Exact masses of the samples were determined by a Mettler balance with precision of 5×10^{-5} g.

The temperature of the calorimeter was registered by means of Fe–Rh resistance thermometer ($R_{273.1} \approx 50\ \Omega$) with a sensitivity of ±0.005 K. The temperature gradient between container and adiabatic shield was controlled with four-junction (Cu + 0.1 wt% Fe)-Chromel thermocouple with a sensitivity of ±0.003 K. The performance of the calorimeter was tested with a high-purity Cu (0.99995 mass fraction) and chromatographically pure *n*-heptane. Maximum deviation of the experimental data from the literature data[22,23] did not exceed 0.3% above 80 K. The error of the container temperature determination was estimated as ±0.02 K within the whole range of temperatures (80–370 K).

The reproducibility of the results was confirmed by repeated measurements of the heat capacity curve. The results of these measurements were found to coincide with each other within the experimental error of the instrument employed.

2.5. High-temperature calorimetry

All calorimetric measurements in the temperature range between 373 and 1273 K were performed with MHTC 96 drop calorimeter (Setaram, France). Enthalpy increments for Sr_2CoMoO_6 and Sr_2NiMoO_6 were determined by dropping the small dense chunks (around 50 mg) of oxide from room temperature to the platinum crucible installed in the calorimetric cell which was heated to high temperature. The reproducibility of the enthalpy increments' measurements was found to be less than 2% up to 1273 K.

In order to obtain the formation enthalpies, smaller amounts (10–20 mg) of oxides and precursors were dissolved in alkali-metal borate melt. Around 6.5 g of equimolar mixture of sodium and lithium metaborates with general formula $NaLi(BO_2)_2$ was used as a solvent. The complex oxide Sr_2CoMoO_6 and its precursors (CoO, MoO_3 and $SrCO_3$) were dissolved in borate melt at 1073 K. However, NiO and Sr_2NiMoO_6 did not dissolve rapidly at this temperature, so drop solution experiments for these oxides as well as MoO_3 and $SrCO_3$ were conducted at 1173 K. At least 6 measurements were performed for each sample at each high temperature investigated in either drop or drop solution experiments.

The calorimeter was calibrated during each experiment by successive dropping of the sample and standard material into the calorimetric cell. High-purity sapphire (NIST SRM 720) and gold (99.99%) were used as standard materials for drop and drop solution experiments, respectively. The thermodynamic functions for sapphire were obtained from the NIST certificate, and for gold – from the work of Arblaster.[24] The masses of sapphire cylinders and gold beads that were used for calibration were 30–40 mg and 50–70 mg, respectively.

Average atmospheric pressure during all calorimetric measurements was 1015 ± 5 mbar.

3. Results and discussion

3.1. Heat of formation

As the oxygen nonstoichiometry in both Sr_2CoMoO_6 and Sr_2NiMoO_6 is expected to be very small in air,[13,15] their nominal (stoichiometric) compositions were used in the present work. The values of the experimental enthalpies of drop solution in borate melt are shown in Table 2. The uncertainties presented in this table and throughout this work were calculated as doubled standard deviations, corresponding to a level of confidence of approximately 95%. Enthalpy increments for CO_2 gas and the formation enthalpies of oxides, which are necessary to complete the thermochemical cycles, were taken from Robie and Hemingway.[25]

Calculated standard enthalpies of formation of Sr_2CoMoO_6 and Sr_2NiMoO_6 from oxides and elements are shown in Table 3. As seen, the standard formation enthalpies of both double perovskites are equal to each other within the estimated uncertainty intervals.

3.2. Heat capacity curves and phase transitions

Experimental values of heat capacity of Sr_2CoMoO_6 and Sr_2NiMoO_6 are shown in Fig. 2 along with the data of Gunjikar *et al.*[18] Original experimental data on both heat capacity and high-temperature enthalpy increments are given in ESI.† It is clearly seen in the inset in Fig. 2 that, despite much higher experimental error for C_p determination with PPMS, in the temperature range 80–100 K, where the measurement points overlap, there is an excellent

Table 2 Experimental standard enthalpies of drop solution and related calorimetric data necessary for the calculation of the formation enthalpies of Sr_2CoMoO_6 and Sr_2NiMoO_6

i	Reaction	ΔH_i^0, kJ mol^{-1}
1	$SrCO_3$ (s, 298 K) → SrO (sol, 1073 K) + CO_2 (g, 1073 K)	261.9 ± 3.7
2	$SrCO_3$ (s, 298 K) → SrO (sol, 1173 K) + CO_2 (g, 1173 K)	276.7 ± 3.4
3[a]	CO_2 (g, 298 K) → CO_2 (g, 1073 K)	37.40
4[a]	CO_2 (g, 298 K) → CO_2 (g, 1173 K)	42.96
5[a]	SrO (s, 298 K) + CO_2 (g, 298 K) → $SrCO_3$ (s, 298 K) $\Delta H_5 = \Delta_f H^0(SrCO_3) - \Delta_f H^0(SrO) - \Delta_f H^0(CO_2)$	−233.9 ± 1.8
6	MoO_3 (s, 298 K) → MoO_3 (sol, 1073 K)	−7.6 ± 0.5
7	MoO_3 (s, 298 K) → MoO_3 (sol, 1173 K)	7.8 ± 1.3
8	CoO (s, 298 K) → CoO (sol, 1073 K)	90.8 ± 1.8
9	NiO (s, 298 K) → NiO (sol, 1173 K)	90.9 ± 1.8
10	Sr_2CoMoO_6 (s, 298 K) → 2SrO (sol, 1073 K) + CoO (sol, 1073 K) + MoO_3 (sol, 1073 K)	321.6 ± 3.8
11	Sr_2NiMoO_6 (s, 298 K) → 2SrO (sol, 1173 K) + NiO (sol, 1173 K) + MoO_3 (sol, 1173 K)	349.4 ± 9.3

s – solid, sol – solution in $NaLi(BO_2)_2$, g – gas.[a] Data from Robie and Hemingway.[25]

Table 3 Calculation of the standard enthalpies of formation of Sr_2CoMoO_6 and Sr_2NiMoO_6 from oxides and elements

	$\Delta_f H^0$, kJ mol^{-1}
2SrO (s, 298 K) + CoO (s, 298 K) + MoO_3 (s, 298 K) → Sr_2CoMoO_6 (s, 298 K) $\Delta_{f,ox}H^0(Sr_2CoMoO_6) = 2(\Delta H_1 + \Delta H_5 - \Delta H_3) + \Delta H_6 + \Delta H_8 - \Delta H_{10}$	−257.2 ± 9.3
2SrO (s, 298 K) + NiO (s, 298 K) + MoO_3 (s, 298 K) → Sr_2NiMoO_6 (s, 298 K) $\Delta_{f,ox}H^0(Sr_2NiMoO_6) = 2(\Delta H_2 + \Delta H_5 - \Delta H_4) + \Delta H_7 + \Delta H_9 - \Delta H_{11}$	−251.0 ± 12.3
$\Delta_f H^0(Sr_2CoMoO_6) = \Delta_{f,ox}H^0(Sr_2CoMoO_6) + 2\Delta_f H^0(SrO) + \Delta_f H^0(CoO) + \Delta_f H^0(MoO_3)$	−2422.9 ± 9.6
$\Delta_f H^0(Sr_2NiMoO_6) = \Delta_{f,ox}H^0(Sr_2NiMoO_6) + 2\Delta_f H^0(SrO) + \Delta_f H^0(NiO) + \Delta_f H^0(MoO_3)$	−2418.1 ± 12.4

agreement between the data measured by adiabatic and relaxation calorimetry.

For each of the double perovskites a good coincidence between two data sets within the corresponding error margins is observed in Fig. 2 in the temperature range between 300 and 370 K, where both our and literature data[18] exist. However, as it will be explained below, the peaks in C_p found by Gunjikar *et al.*[18] are doubtful and should be due to some kind of an experimental error.

Each of Sr_2CoMoO_6 and Sr_2NiMoO_6 oxides exhibits two phase transitions in the temperature region from 0 to 1273 K. The first one that occurs at lower temperatures, as it was pointed out in literature,[3–9,11,26] is a second-order antiferromagnetic (AFM) phase transition. Indeed, distinct lambda-shaped regions are clearly seen on specific heat dependencies given in Fig. 2. The temperatures of local maxima of $C_p(T)$ within these regions correspond to the phase transition temperatures and presented in Table 4. As seen, the values of the transition temperatures found in the present study are close to some of those previously reported.[3,4]

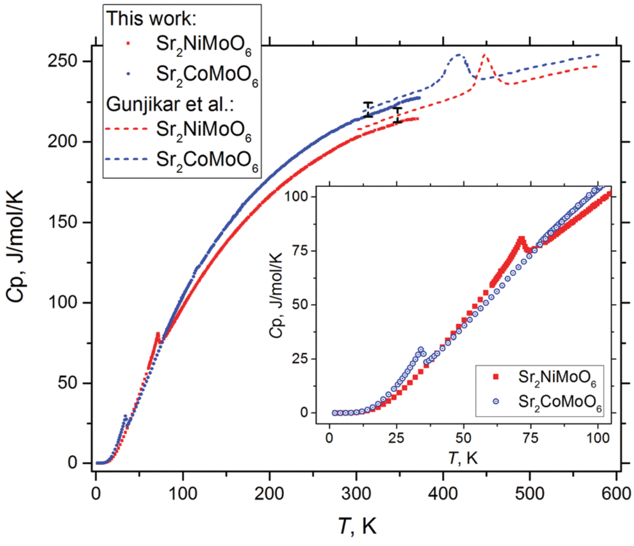

Fig. 2 Specific heat of Sr_2CoMoO_6 and Sr_2NiMoO_6: original data and those of Gunjikar *et al.*[18]

The second, high-temperature transition, which is deemed to be an improper ferroelectric phase transition,[10] is accompanied by the crystal lattice symmetry change from tetragonal ($I4/m$) to cubic ($Fm\bar{3}m$). This symmetry change is due to the slight rotation of the MO_6 (M = Ni, Co) and MoO_6 octahedra.[6,7,15] In contrast with the AFM phase transition, which is undoubtedly one of a second order, there are several works where physical value changes that are characteristic of the first-order phase transition were pointed out. In particular, Wei *et al.*[16] asserted that a peak at around 495 K exists on thermal expansion coefficient (TEC) curve for Sr_2NiMoO_6, though the relative expansion curve presented in their paper[16] looks smooth, and no TEC curve is given to confirm their assertion. Filonova and Dmitriev[30] reported the sharp volume increase for the same oxide at 508 K, as obtained as a result of XRD refinement. However, this finding was not confirmed by authors' own dilatometric measurements and, moreover, it contradict the findings of other authors who did not detect any abnormal volume change upon the symmetry change for either Sr_2CoMoO_6 or Sr_2NiMoO_6.[3,15,16,27,31] Finally, Gunjikar *et al.*[18] described significant humps on specific heat *vs.* temperature curves at around 417 and 452 K for Sr_2CoMoO_6 or Sr_2NiMoO_6, respectively.

Table 4 Temperatures (in K) of phase transitions in Sr_2CoMoO_6 and Sr_2NiMoO_6 along with the properties or methods used for their determination

Phase transition	Sr_2NiMoO_6	Sr_2CoMoO_6
Antiferromagnetic phase transition	71.8 (present work, heat capacity) 71.5[3] (magnetic susceptibility) 80[7,9] (magnetic susceptibility) 81.2[26] (NPD[a])	34.5 (present work, heat capacity) 34[4] (magnetic susceptibility) 36[6] (magnetic susceptibility) 37[5,8,9,11] (magnetic susceptibility)
$I4/m \rightarrow Fm\bar{3}m$	463[10] (dielectric permittivity) 503[3] (resistivity, magnetic susceptibility) 538[15] (XRD) 523–573[27] (XRD) 550–575[7] (NPD) 553[28] (dielectric permittivity)	447[29] (NPD, heating) 535[29] (NPD, cooling) 560[6] (dielectric permittivity) 563[10] (dielectric permittivity) 628[15] (XRD)

[a] NPD – Neutron powder diffraction.

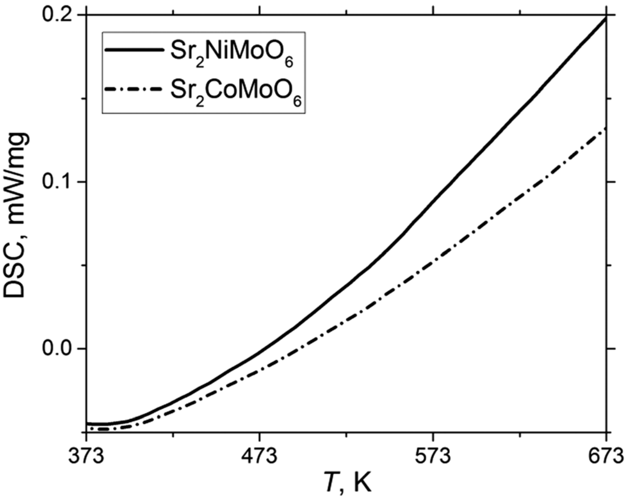

Fig. 3 DSC curves for Sr_2CoMoO_6 and Sr_2NiMoO_6.

However, DSC results obtained in the present study are in a perfect agreement with those of Zheng and Świerczek[15] and confirm that the structural $I4/m \rightarrow Fm\bar{3}m$ phase transitions in Sr_2CoMoO_6 and Sr_2NiMoO_6 are not accompanied by any heat effects (see Fig. 3). Thus, the said transition should be of a second order. In this respect, the findings of Wei *et al.*,[16] Filonova and Dmitriev,[30] and Gunjikar *et al.*[18] seem to be somewhat doubtful, and, therefore, are not included in Table 4.

By definition, there is no latent heat associated with $I4/m \rightarrow Fm\bar{3}m$ second-order phase transformation. No anomalies, such as the change in slope of DSC curve or the change in the enthalpy increments' trends, were detected for both double perovskites around the supposed phase transition temperatures (see Table 4 and Fig. 3). Additionally, quite a large scatter in reported temperatures of the structural phase transition for Sr_2CoMoO_6 and Sr_2NiMoO_6 can be pointed out. It can be related to the continuous nature of this transformation, when properties of the oxide are changing so gradually upon heating that it is hard to pinpoint the exact transition temperature. Therefore, we assume that the differences between the thermochemical properties of either Sr_2CoMoO_6 or Sr_2NiMoO_6 with different crystal structure are small enough and, therefore, can be ignored. As a consequence, we do not make distinctions between the thermodynamic functions of high-temperature tetragonal and cubic phases of each of the double perovskites studied in the present work.

3.3. Heat capacity and thermodynamic functions

Specific heat functions for Sr_2CoMoO_6 and Sr_2NiMoO_6 in the whole temperature range investigated (from 2 to 1273 K) can be approximated using the approach developed by Voronin and Kutsenok,[32] as implemented in CpFit v. 0.7 software.[33] The major advantage of this approach over the other methods of heat capacity approximation is that it allows simultaneous fitting of $C_p(T)$ functions to both low-temperature (specific heat) and high-temperature (enthalpy increments) experimental data, ensuring the smooth transition and good correspondence between below- and above-room-temperature regions of $C_p(T)$. In the method of Voronin and Kutsenok,[32] $C_p(T)$ function is represented by the weighted sum of Einstein terms with different Einstein temperatures. In turn, the low-temperature second-order phase transition can be described by two exponentials which are then added to the said sum. Hence, a piecewise $C_p(T)$ function for Sr_2CoMoO_6 and Sr_2NiMoO_6 can be expressed as

$$C_p(T) = \sum_{i=1}^{j}\left(\alpha_i \cdot \frac{3Rx^2\exp(x)}{(\exp(x)-1)^2}\right) + \begin{cases} mRT\exp(n(T-T_{\max})), & T \le T_{\max} \\ bRT\exp(-q(T-T_{\max})), & T > T_{\max} \end{cases}, \tag{1}$$

where α_i is a weight of the corresponding Einstein term, $x = \theta_i/T$, θ_i is Einstein temperature, $T_{\max}$ is a phase transition temperature (*i.e.* T where C_p attains local maximum), and m, n, b and q are the fitting parameters for the exponentials. The values of $\Delta_0^T H^0 = (H^0(T) - H^0(0))$ and $S^0(T)$ can be found by integrating (1) with respect to T and $\ln T$ according to the well-known relations.

All unknown parameters in the eqn (1), except $T_{\max}$ which was arbitrarily chosen, were found during the fitting procedure and are listed in Table 5. It is seen that for most of the parameters expanded uncertainties, estimated during the Levenberg–Marquardt fitting, are quite small. As shown in Fig. 4, the deviations of fitted $C_p(T)$ dependencies from the experimental values are well within 2% for most of the temperature range, exceeding this margin only at the lowest temperatures, where the absolute experimental error itself is the greatest. The corresponding deviations for the enthalpy increments, plotted in Fig. 5, do not exceed several percent as well.

The smoothed values of $C_p(T)$, $\Delta_0^T H^0(T)$ and $S^0(T)$ for Sr_2CoMoO_6 and Sr_2NiMoO_6, calculated using the corresponding functional dependencies derived from (1), are presented in Table 6. For the ease of use, the specific heat, enthalpy and entropy functions for both double perovskites with coefficients substituted from Table 5 are given in ESI.†

It's interesting to note that in case of Sr_2CoMoO_6 and Sr_2NiMoO_6, Neumann–Kopp's rule fails to predict an accurate value of C_p at room temperature. The reference values[25] of heat capacity for SrO, CoO, MoO_3 and NiO were taken for empirical heat capacity estimation. For nickel-containing double perovskite the value predicted (210.2 J mol^{-1} K^{-1}) is almost 4% lower than the experimental one. For Sr_2CoMoO_6, the value of 209.1 J mol^{-1} K^{-1} is fairly close to the experimental one. However, in the majority of thermodynamic data sources (see, for example, Barin[34]) the heat capacity of CoO at 298.15 K is more than 20% larger than the one presented by Robie and Hemingway,[25] while heat capacities of the other oxides are comparable. Taking the higher value of C_p(CoO) for the calculation leads to around 4% overestimation of the predicted specific heat value for Sr_2CoMoO_6.

Table 5 Fitting parameters for $C_p(T)$ approximating functions (1) for Sr_2CoMoO_6 and Sr_2NiMoO_6

	Sr_2NiMoO_6		Sr_2CoMoO_6	
Parameter	Value	Expanded uncertainty	Value	Expanded uncertainty
α_1	4.949	0.047	5.314	0.119
α_2	3.676	0.048	3.308	0.123
α_3	1.296	0.064	1.745	0.049
α_4	3.634×10^{-2}	0.213×10^{-2}	7.084×10^{-2}	0.639×10^{-2}
α_5	5.389×10^{-4}	0.159×10^{-4}	9.440×10^{-4}	0.201×10^{-4}
θ_1	673.60	7.33	317.01	6.24
θ_2	225.82	3.50	794.55	28.91
θ_3	116.44	1.46	112.14	1.09
θ_4	46.33	0.65	55.42	0.96
θ_5	7.48	0.14	4.26	0.17
T_{max}	71.8	—	34.5	—
m	1.911×10^{-2}	0.083×10^{-2}	3.562×10^{-2}	0.403×10^{-2}
n	1.276×10^{-1}	0.063×10^{-1}	1.874×10^{-1}	0.159×10^{-1}
b	1.884×10^{-2}	0.350×10^{-2}	1.123×10^{-1}	0.488×10^{-1}
q	7.162×10^{-1}	0.574×10^{-1}	3.776	0.394

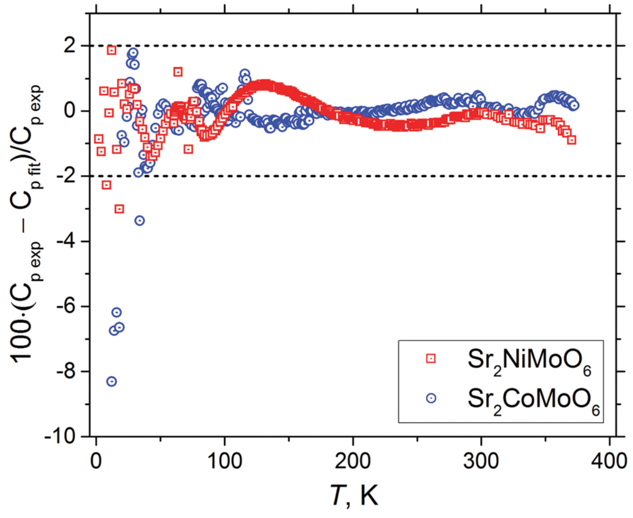

Fig. 4 Percental deviations of fitted specific heat functions from experimental values.

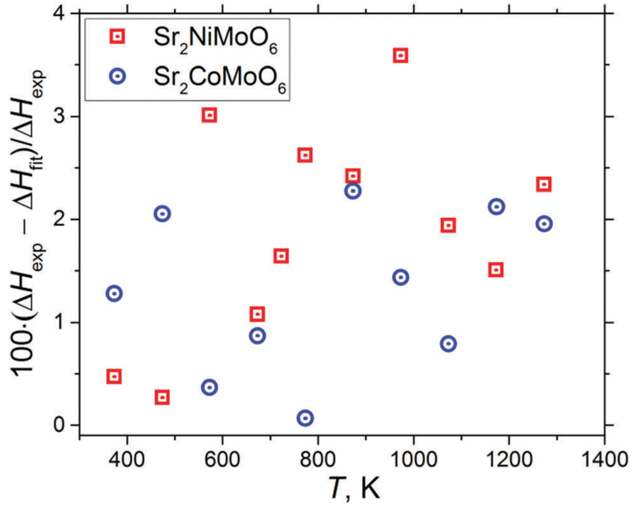

Fig. 5 Percental deviations of fitted enthalpy increment functions from experimental values.

Surprisingly good prediction of S^0_{298} of Sr_2NiMoO_6 and Sr_2CoMoO_6 can be made on the basis of Kelley's additive scheme. In this method, the increments for individual ions should be added together to get the value of standard entropy of an inorganic compound. The table with corresponding entropy increments is given in the ESI.† In addition, knowledge about the low-temperature antiferromagnetic phase transition in both double perovskites allows us to take into account the magnetic entropy contribution.[35] Thus, the value of S^0_{298} can be approximated as

$$S^0_{298} = S^0_{\text{Kelley}} + S^0_{\text{magn}} = S^0_{\text{Kelley}} + R\ln(2s + 1), \qquad (2)$$

where s is a spin of magnetic cation (Co or Ni). Values of S^0_{298}, calculated accordingly, are 228.35 and 242.18 J mol^{-1} K^{-1} for Sr_2NiMoO_6 and Sr_2CoMoO_6, respectively, showing less than 1.5% deviations from the experimental values.

Table 7 shows the values of standard entropy and Gibbs energy of formation along with the measured standard enthalpies of formation for both double perovskites investigated. For $\Delta_f S^0_{298}$ calculation, the values of standard entropy for elements in their most stable states were taken from Robie and Hemingway.[25]

3.4. Stability calculations

The available thermodynamic data allowed us to evaluate the thermodynamic stability of the double perovskites Sr_2NiMoO_6 and Sr_2CoMoO_6. It was done by minimizing the total Gibbs

Table 6 Smoothed standard thermodynamic functions of Sr_2NiMoO_6 and Sr_2CoMoO_6 *vs.* temperature. Estimated expanded uncertainties below 80 K are 0.02·*x*, where *x* represents a thermodynamic property, and $0.003 \cdot C_p$, $0.005 \cdot \Delta_0^T H^0$ and $0.007 \cdot S^0$ for higher temperatures

	Sr_2NiMoO_6			Sr_2CoMoO_6		
T, K	C_p, J mol^{-1} K^{-1}	$\Delta_0^T H^0$, J mol^{-1}	S^0, J mol^{-1} K^{-1}	C_p, J mol^{-1} K^{-1}	$\Delta_0^T H^0$, J mol^{-1}	S^0, J mol^{-1} K^{-1}
0	0.00	0.00	0.00	0.00	0.00	0.00
10	0.24	0.54	0.07	0.34	0.71	0.11
25	8.39	46.68	2.36	12.63	73.51	3.74
50	43.24	666.54	18.15	40.15	711.93	20.20
75	75.16	2158.29	41.85	73.80	2134.58	42.81
100	97.44	4312.53	66.48	103.79	4367.41	68.30
125	117.87	7007.98	90.46	127.89	7274.25	94.14
150	136.39	10190.43	113.62	147.58	10725.45	119.26
175	152.70	13808.95	135.90	163.94	14625.57	143.27
200	166.64	17805.69	157.22	177.61	18900.04	166.08
225	178.33	22122.28	177.55	189.01	23487.09	187.68
250	188.03	26705.60	196.85	198.52	28334.86	208.10
273.15	195.53	31147.92	213.84	205.92	33018.69	226.02
275	196.08	31510.16	215.16	206.46	33400.15	227.41
298.15	202.31	36123.54	231.27	212.66	38253.40	244.35
300	202.76	36498.23	232.52	213.11	38647.24	245.67
350	213.01	46907.39	264.59	223.42	49574.89	279.34
400	220.30	57749.91	293.54	230.85	60941.37	309.68
450	225.62	68904.61	319.81	236.33	72627.72	337.20
500	229.60	80289.86	343.79	240.47	84552.47	362.33
550	232.65	91849.36	365.83	243.65	96658.72	385.40
600	235.02	103543.37	386.18	246.14	108905.83	406.71
650	236.90	115343.12	405.06	248.12	121264.18	426.50
700	238.42	127227.39	422.68	249.73	133711.74	444.94
750	239.65	139180.19	439.17	251.04	146231.85	462.22
800	240.68	151189.29	454.67	252.12	158811.71	478.46
850	241.53	163245.17	469.29	253.03	171441.30	493.77
900	242.25	175340.32	483.12	253.80	184112.72	508.26
950	242.87	187468.75	496.23	254.46	196819.62	522.00
1000	243.39	199625.63	508.70	255.02	209556.90	535.06
1050	243.85	211806.99	520.59	255.51	222320.34	547.52
1100	244.25	224009.58	531.94	255.93	235106.49	559.41
1150	244.59	236230.69	542.81	256.30	247912.47	570.80
1200	244.90	248468.06	553.22	256.63	260735.86	581.71
1250	245.17	260719.76	563.23	256.92	273574.62	592.20

Table 7 Standard enthalpy, entropy and Gibbs energy of formation of Sr_2NiMoO_6 and Sr_2CoMoO_6 at 298.15 K

Compound	$\Delta_f H^0_{298}$, kJ mol^{-1}	$\Delta_f S^0_{298}$, J mol^{-1} K^{-1}	$\Delta_f G^0_{298}$, kJ mol^{-1}
Sr_2NiMoO_6	−2418.1 ± 12.4	−554.1 ± 3.9	−2252.9 ± 12.5
Sr_2CoMoO_6	−2422.9 ± 9.6	−541.2 ± 3.8	−2261.5 ± 9.6

energy of a system consisting of solid metals, oxides and molybdates, and oxygen in the gaseous phase:

$$G(T, p_{O_2}) = RT \ln p_{O_2} + \sum_i x_i G_i^0(T), \qquad (3)$$

where x_i represents the quantity of the phase i with standard Gibbs energy function $G_i^0(T) = \Delta_f H^0(T) - TS^0(T)$. Additionally, the conditions of mass balance were imposed as constraints during the minimization, ensuring that the system should contain an excess of oxygen and stoichiometric quantities of other elements, *i.e.*

$$n(\mathrm{Sr}) : n(\mathrm{M}) : n(\mathrm{Mo}) = 2:1:1, \qquad (4)$$

where M is either Co or Ni.

When the exact $G^0(T)$ functions are known for any probable phase in the system, a simple form of calculation of phase diagrams (CALPHAD) approach[35] can be implemented in the mathematical software of choice, which in our case was Maple (Maplesoft, Canada). Thermodynamic data for gaseous O_2, CO_2, and Sr, and solid NiO, SrO, CoO, Co_3O_4, Co, Ni, Mo, Cr, Cr_2O_3, and $SrCO_3$ were taken from the well-known database of Gurvich[36] and Iorish.[37] Some of these data, in order to obtain self-consistent thermodynamic data set, were used to calculate $G^0(T)$ functions from the original experimental results on various strontium molybdates: $SrMoO_3$,[38] $SrMoO_4$,[39,40] Sr_3MoO_6[41] and Sr_2MoO_4.[39] Phase diagrams for Sr_2NiMoO_6 and Sr_2CoMoO_6, obtained as a result of a mapping procedure, *i.e.* by calculating the composition of a system in a set of (T, p_{O_2}) points, are shown in Fig. 6 and 7, respectively.

As seen in Fig. 6 and 7 the decomposition routes of Sr_2NiMoO_6 and Sr_2CoMoO_6 are essentially similar at lower p_{O_2}. Following the p_{O_2} decrease, single-phase double perovskite transforms into metallic Ni or Co and the mixture of strontium molybdates Sr_3MoO_6 and $SrMoO_4$. Further decrease of p_{O_2} leads to the reduction of $SrMoO_4$ to $SrMoO_3$, followed by the decomposition of Sr_3MoO_6 into $SrMoO_3$ and SrO under more reducing conditions. At temperatures higher than around 1310 K the mixture of $SrMoO_3$ and SrO forms Sr_2MoO_4.

Mentioned in the Introduction variety in the products of Sr_2NiMoO_6 and Sr_2CoMoO_6 reduction[9,11,12,14,17] can be easily

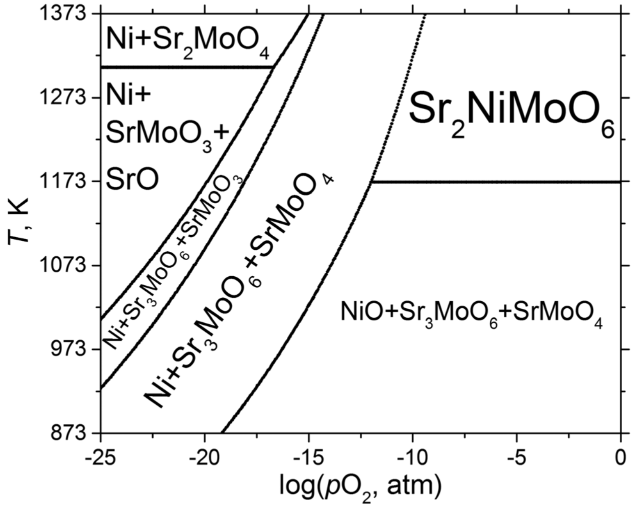

Fig. 6 Equilibrium phase diagram of Sr_2NiMoO_6.

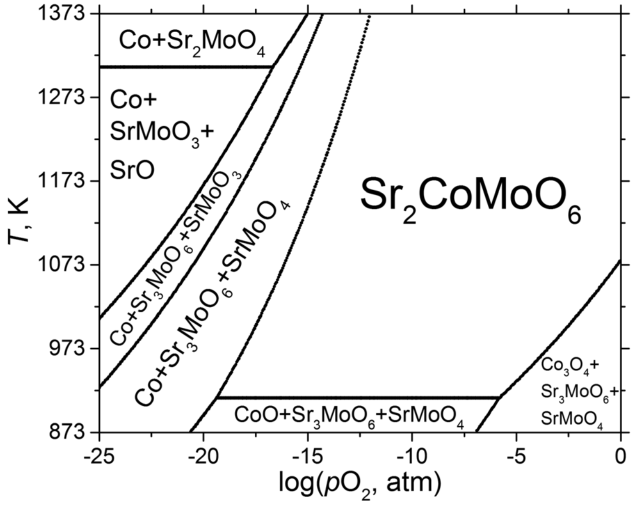

Fig. 7 Equilibrium phase diagram of Sr_2CoMoO_6.

understood now. Multiple reasons might be responsible for that. As seen in Fig. 6 and 7, different strontium molybdates coexist within the fields on the phase diagrams, and the p_{O_2} ranges in which the particular mixture of strontium molybdates with metallic Co or Ni is stable are rather narrow. Taking into account that the value of p_{O_2} in H_2/inert gas mixture depends strongly on its humidity because of the well-known H_2/H_2O equilibrium, precise humidity or p_{O_2} control is required during the reduction experiment in order to obtain the particular mixture of decomposition products. Besides, the identification of the reduction products often implies cooling the partially or completely reduced samples down to the room temperature, which could lead to the oxidation of some strontium molybdates, for example, $SrMoO_3$ to $SrMoO_4$. The variability of cooling rates complicates the issue further. Additional considerations should be given to the duration of annealing under reducing conditions, because the decomposition of Sr_2NiMoO_6 and Sr_2CoMoO_6 might be kinetically hindered.

As it follows from comparison of Fig. 6 and 7, decomposition of Sr_2NiMoO_6 and Sr_2CoMoO_6 differs at lower temperatures and higher p_{O_2} primarily because of the possibility of Co_3O_4 exsolution from the latter double perovskite. Namely, the formation of stable Co_3O_4 leads to the increase in temperature of Sr_2CoMoO_6 decomposition at higher oxygen partial pressures (see Fig. 7). Nevertheless, Sr_2CoMoO_6 has significantly wider range of stability with respect to both T and p_{O_2} than Sr_2NiMoO_6. While both Sr_2NiMoO_6 and Sr_2CoMoO_6 are unstable at low temperatures and/or low oxygen partial pressures, the existence of metastable single-phase Sr_2NiMoO_6 or Sr_2CoMoO_6 at low temperatures is possible because of the sluggish rate of decomposition of these double perovskites due to aforementioned kinetic limitations.

4. Conclusions

Using the experimental data measured by low-temperature relaxation calorimetry, adiabatic calorimetry and high-temperature drop calorimetry, $C_p(T)$ dependencies were obtained for Sr_2NiMoO_6 and Sr_2CoMoO_6 in the broad temperature range, from 2 to 1273 K. Standard enthalpy $\Delta_0^T H^0(T)$ and entropy $S^0(T)$ functions were derived from $C_p(T)$ for both double perovskites. Additional data on $\Delta_f H_{298}^0$, obtained by the high-temperature drop solution calorimetry, completed the whole set of essential thermodynamic properties for Sr_2NiMoO_6 and Sr_2CoMoO_6. It allowed us to derive $G^0(T)$ functions and use them along with the literature data to construct the phase diagrams for both oxides with respect to T and p_{O_2}. As expected, the thermodynamic approach works well and predicts unambiguously the stability limits of compounds in question.

Conflicts of interest

There are no conflicts of interest to declare.

Acknowledgements

This work was supported by Russian Foundation for Basic Research (Grant No. 15-33-20978).

References

1 S. Vasala and M. Karppinen, *Prog. Solid State Chem.*, 2015, **43**, 1–36.
2 L. H. Brixner, *J. Phys. Chem.*, 1960, **64**, 165–166.
3 S. Nomura and T. Nakagawa, *J. Phys. Soc. Jpn.*, 1966, **21**, 1068–1071.
4 M. Itoh, I. Ohta and Y. Inaguma, *Mater. Sci. Eng., B*, 1996, **41**, 55–58.
5 M. C. Viola, M. J. Martínez-Lope, J. A. Alonso, P. Velasco, J. L. Martínez, J. C. Pedregosa, R. E. Carbonio and M. T. Fernández-Díaz, *Chem. Mater.*, 2002, **14**, 812–818.
6 S. A. Ivanov, S. G. Eriksson, R. Tellgren, H. Rundlöf and M. Tseggai, *Mater. Res. Bull.*, 2005, **40**, 840–849.

7 A. K. Eriksson, S. G. Eriksson, S. A. Ivanov, C. S. Knee, J. Eriksen, H. Rundlöf and M. Tseggai, *Mater. Res. Bull.*, 2006, **41**, 144–157.

8 A. Azizi, A. Kahoul, G. Schmerber, S. Colis and A. Dinia, *Int. J. Mod. Phys. B*, 2008, **22**, 3579–3588.

9 Y.-H. Huang, G. Liang, M. Croft, M. Lehtimäki, M. Karppinen and J. B. Goodenough, *Chem. Mater.*, 2009, **21**, 2319–2326.

10 V. V. Gagulin, S. K. Korchagina, V. V. Ivanova and Y. A. Shevchuk, *Inorg. Mater.*, 2003, **39**, 625–626.

11 P. Zhang, Y.-H. Huang, J.-G. Cheng, Z.-Q. Mao and J. B. Goodenough, *J. Power Sources*, 2011, **196**, 1738–1743.

12 C. Graves, B. R. Sudireddy and M. Mogensen, *ECS Trans.*, 2010, **28**, 173–192.

13 S. Vasala, M. Lehtimäki, Y. H. Huang, H. Yamauchi, J. B. Goodenough and M. Karppinen, *J. Solid State Chem.*, 2010, **183**, 1007–1012.

14 L. dos Santos-Gómez, L. León-Reina, J. M. Porras-Vázquez, E. R. Losilla and D. Marrero-López, *Solid State Ionics*, 2013, **239**, 1–7.

15 K. Zheng and K. Świerczek, *J. Eur. Ceram. Soc.*, 2014, **34**, 4273–4284.

16 T. Wei, Y. Ji, X. Meng and Y. Zhang, *Electrochem. Commun.*, 2008, **10**, 1369–1372.

17 K. Zheng, K. Świerczek, W. Zając and A. Klimkowicz, *Solid State Ionics*, 2014, **257**, 9–16.

18 V. G. Gunjikar, N. Ramachandran and H. V. Kehr, *J. Indian Chem. Soc.*, 1982, **59**, 743–744.

19 A. Navrotsky, *Phys. Chem. Miner.*, 1997, **24**, 222–241.

20 J. J. Lander, *J. Am. Chem. Soc.*, 1951, **73**, 5794–5797.

21 R. M. Varushchenko, A. I. Druzhinina and E. L. Sorkin, *J. Chem. Thermodyn.*, 1997, **29**, 623–637.

22 R. Stevens and J. Boerio-Goates, *J. Chem. Thermodyn.*, 2004, **36**, 857–863.

23 T. B. Douglas, G. T. Furukawa, R. E. McCoskey and A. F. Ball, *J. Res. Natl. Bur. Stand.*, 1954, **54**, 139–153.

24 J. W. Arblaster, *J. Phase Equilib. Diffus.*, 2016, **37**, 229–245.

25 R. A. Robie and B. S. Hemingway, *Thermodynamic properties of minerals and related substances at 298.15 K and 1 bar (10 Pascals) pressure and at higher temperatures*, U.S. goverment printing office, Washington, 1995.

26 María J. Martínez-Lope, José A. Alonso and María T. Casais, *Eur. J. Inorg. Chem.*, 2003, 2839–2844.

27 W. L. Michael, B. M. René, L. Yongjae, V. Thomas and L. Hans-Conrad zur, *J. Phys.: Condens. Matter*, 2006, **18**, 8761.

28 A. Prasatkhetragarn, S. Kaowphong and R. Yimnirun, *Appl. Phys. A: Mater. Sci. Process.*, 2012, **107**, 117–121.

29 A. Aguadero, J. A. Alonso, R. Martínez-Coronado, M. J. Martínez-Lope and M. T. Fernández-Díaz, *J. Appl. Phys.*, 2011, **109**, 034907.

30 E. A. Filonova and A. S. Dmitriev, *Eurasian Chem. – Technolo. J.*, 2012, **14**, 139–145.

31 P. Kumar, N. K. Singh, R. K. Singh and P. Singh, *Appl. Phys. A*, 2015, **121**, 635–644.

32 G. F. Voronin and I. B. Kutsenok, *J. Chem. Eng. Data*, 2013, **58**, 2083–2094.

33 A. L. Voskov, I. B. Kutsenok and G. F. Voronin, *CALPHAD: Comput. Coupling Phase Diagrams Thermochem.*, 2018, **61**, 50–61.

34 I. Barin, *Thermochemical Data of Pure Substances*, VCH Verlagsgesellschaft mbH, 3rd edn, 1995.

35 N. Saunders and A. P. Miodownik, *CALPHAD (Calculation of Phase Diagrams): A Comprehensive Guide*, Pergamon, 1998.

36 L. V. Gurvich, *Thermodynamic properties of individual substances*, Hemisphere Publishing Corp., New York, 4th edn, 1989.

37 V. S. Iorish, Thermodynamic properties of individual substances (Zn, Cu, Fe, Co, Ni, Mn, Cr, V), http://www.chem.msu.su/rus/tsiv.

38 S. Dash, Z. Singh, R. Prasad and D. D. Sood, *J. Alloys Compd.*, 1993, **201**, 99–102.

39 B. Lindblom and E. Rosén, *Acta Chem. Scand.*, 1986, **40A**, 452–458.

40 Z. Singh, S. Dash, R. Prasad and D. D. Sood, *J. Alloys Compd.*, 1994, **215**, 303–307.

41 Z. Singh, R. Prasad, S. Dash and D. D. Sood, *J. Alloys Compd.*, 1994, **209**, 193–196.